Journal of Engineering Physics and Thermophysics, Vol. 82, No. 4, 2009

EXPERIMENTAL STUDY OF FLUID FLOW AND HEAT TRANSFER FROM A SQUARE PRISM APPROACHING THE WALL OF A WIND TUNNEL

Dipes Chakrabarty[a] and Ranajit Brahma[b]

UDC 536.25

Experimental investigations of fluid flow and heat transfer have been carried out to study the effect of wall proximity due to flow separation around square prisms. Experiments have been carried for Reynolds number equal to $2.6 \cdot 10^4$. The results are presented in the form of pressure coefficient, drag coefficient, and Nusselt numbers for various height ratios, blockage ratios, and angles of attack. The pressure coefficient distribution shows positive values on the front face, whereas on the rear face negative values are observed. The drag coefficient decreases with increase in angle of attack as the height ratio decreases, and its maximum value takes place at an angle of about 50^o. Both the local and average Nusselt numbers decrease as the height ratio decreases.

Keywords: *Flow separation, square prism, blockage ratio, height ratio, angle of attack, pressure coefficient, drag coefficient, Nusselt number.*

Introduction. Many investigations of heat transfer by forced convection near the exterior surface of bluff bodies such as spheres, cylinders, and square, triangular, and rectangular prisms have been carried out. The important characteristics of flow over a bluff body depend on the nature of the boundary layer. As the streamlines pass over a bluff body, separation takes place due to excessive loss of momentum at an adverse pressure gradient from the point which is not far from the leading edge of the body. The study of fluid flow and heat transfer from a bluff body is important in a number of arrangements and fields such as heat exchangers, gas turbine blades, hot wire anemometry and cooling of electronic equipment, vehicle aerodynamics and building aerodynamics. This research is also useful for validation of numerical codes for calculation of complex flows with the huge experimental database on drag force and heat transfer.

From extensive literature search it is revealed that fluid flow over differently shaped bluff bodies like square, triangular, circular, rectangular ones and toroids has been investigated thoroughly [1–8]. Igarashi [5] investigated the flow characteristics around a square prism at an angle of attack $0^o \le \alpha \le 45^o$ in the range of subcritical Reynolds numbers. The flow characteristics can be subdivided according to the magnitude of the angle of attack as: $0^o \le \alpha \le 5^o$ (perfect separation type, symmetric flow); $5^o \le \alpha \le 13^o$ (perfect separation type, unsymmetric flow); $14^o \le \alpha \le 35^o$ (reattachment flow); $35^o \le \alpha \le 45^o$ (wedge flow). The flow pattern is closely related to the rms value of fluctuating pressure. Literature is also available on the study of heat transfer from different geometric shapes of bluff bodies under various conditions like various angles of attack and Reynolds numbers [9–19]. Igarashi [15] studied both the local and average heat transfer from a square prism to an air stream in the range of subcritical Reynolds numbers. He observed that the average heat transfer has a minimum value at an angle of attack α equal to $12–13^o$ and a maximum one at $\alpha = 20–25^o$. From the various sources it is apparent that the experimental investigations of fluid flow and heat transfer in the studies considering the wall effect (i.e., with a varying distance from the wall) with different angles of attack as well as different locations on square prisms have not been adequately covered. In the present work, experimental investigations are carried out to determine the pressure and drag coefficients by measuring the pressure distributions around the square prisms and the average heat transfer rates from the prism as influenced by the angle of attack, blockage ratio, and ratio of the distance of the centroid of the bluff body from the upper wall to the height of the test section in the wind tunnel.

[a]Konkuk University, Department of Mechanical Engineering, Gwannjin-Gu, 1 Hwayang Dong, Seoul-143701, South Korea, email: dipes_chakrabarty@rediffmail.com; [b]Indian Institute of Technology, Department of Mechanical Engineering, Kharagpur-721302, West Bengal, India. Published in Inzhenerno-Fizicheskii Zhurnal, Vol. 82, No. 4, pp. 701–710, July–August, 2009. Original article submitted January 8, 2008; revision submitted July 21, 2008.

1062-0125/09/8204-0697

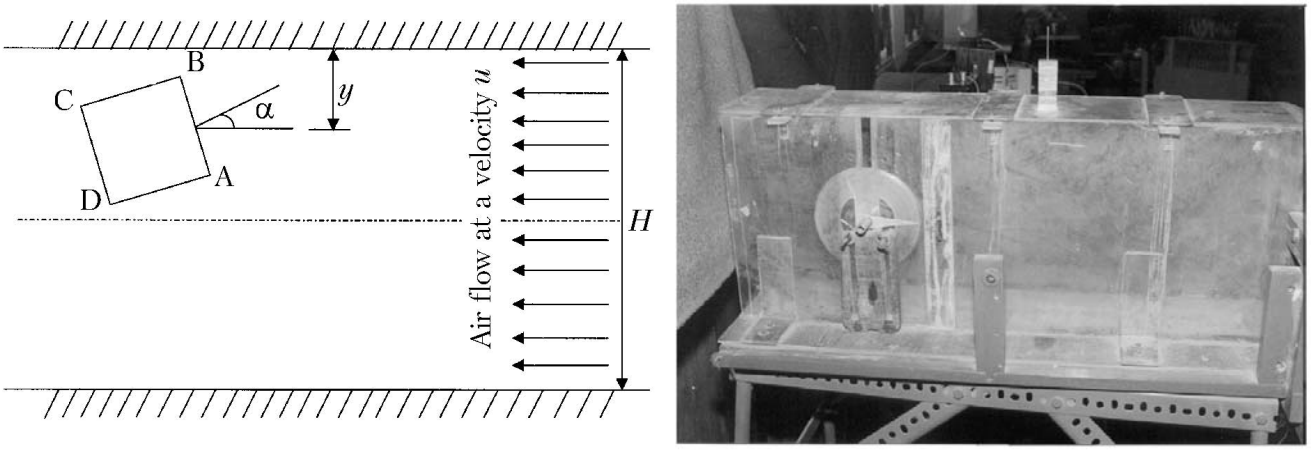

Fig. 1. Schematic diagram of the experimental setup.

Fig. 2. Photograph of the experimental setup.

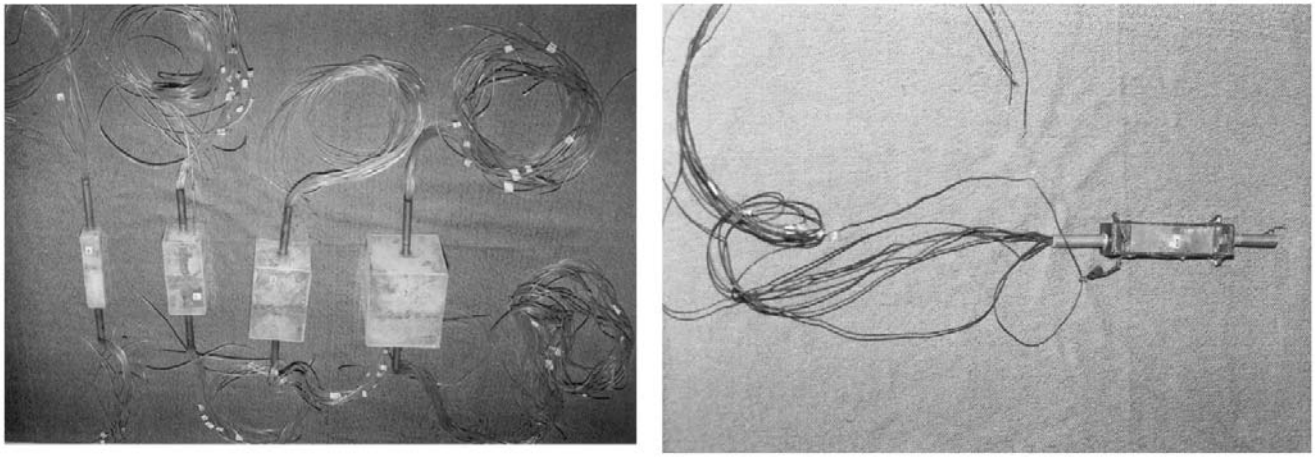

Fig. 3. Photograph of square prisms used in measurement of static pressure distribution.

Fig. 4. Photograph of a square prism used in measurement of heat transfer.

Experimental Technique. The schematic diagram and photograph of the experimental setup are shown in Figs. 1 and 2, respectively. The photographs of the models of square prism for measurement of static pressure distribution and heat transfer are shown in Figs. 3 and 4. The experimental setup consists of a wind tunnel driven by an axial flow fan; the wind tunnel is on the pressure side of the fan and the model is within the test section of the tunnel. The experiment was carried out in a low speed wind tunnel with a working section 300 mm high, 150 mm wide, and 800 mm long. The test model was fitted along the width of the test section. There was a slotting arrangement along the sidewall of the test section of the wind tunnel for lifting the bluff body from the center towards the upper wall of the tunnel to investigate the wall effect on fluid flow and heat transfer characteristics. A Pitot tube measured the approach velocity of the undistributed flow. This tube was placed inside the wind tunnel facing the direction of airflow. A protractor was attached to the bluff body and was fitted at the sidewall of the wind tunnel to measure the angle of rotation of the body. This body rested on the both sides of the sidewall of the tunnel. The square prisms for the fluid flow experiment were made of Perspex sheet 2.5 mm in thickness. The sides of the four prisms were equal to 30, 60, 90, and 120 mm and their length measured 140 mm. Holes numbering of 5, 6, 6, and 4, each 1 mm in diameter, were drilled on each face of the 30, 60, 90, and 120 mm side prisms, respectively, in the mid-span of the prism. The positions of the holes on each face of the prisms were the following: for 30 mm side prism 5, 10, 15, 20,

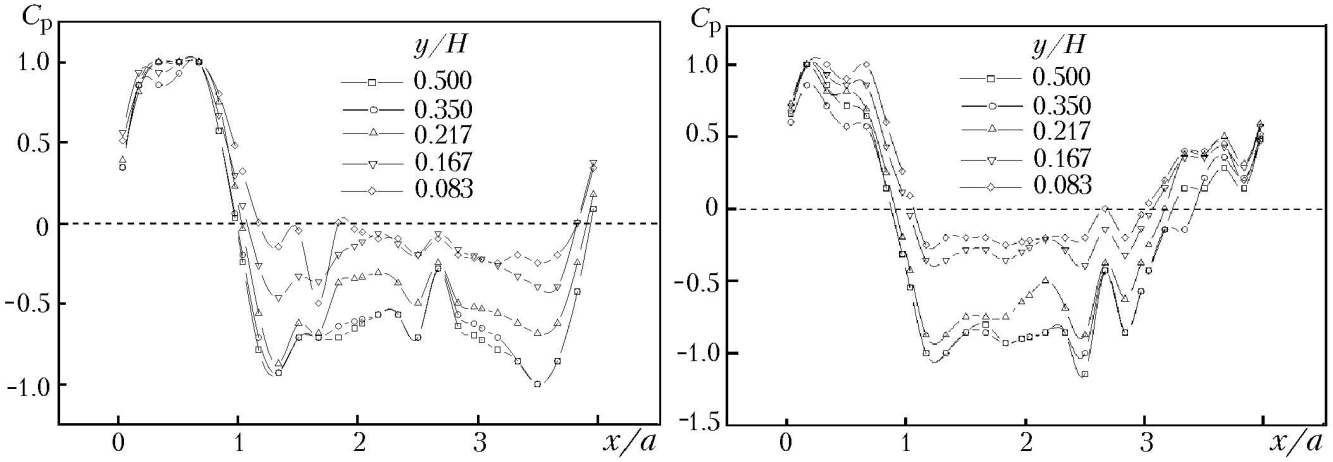

Fig. 5. Variation of pressure coefficient with dimensionless distance at a/H = 0.1, $\alpha = 0^o$, and different height ratios of a square prism.

Fig. 6. Variation of pressure coefficient with dimensionless distance at a/H = 0.1, $\alpha = 30^o$, and different height ratios of a square prism.

25 mm (x/a = 0.167, 0.333, 0.5, 0.667, 0.833); for 60 mm side 5, 15, 25, 35, 45, 55 mm (x/a = 0.083, 0.25, 0.417, 0.583, 0.75, 0917); for 90 mm side 5, 20, 35, 50, 65, 80 mm (x/a = 0.056, 0.222, 0.389, 0.556, 0.722, 0.889); for 120 mm side 5, 35, 80, 110 mm (x/a = 0.042, 0.292, 0.667, 0.917) from the edge of each face. Stainless steel tubes of 1 mm in outside diameter were fitted in tapping and connected with a multitube manometer by flexible tubes for measurement of static pressure distribution. The measurements were made at the following parameters: angle of attack α = 0–85°; blockage ratio a/H = 0.1, 0.2, 0.3, and 0.4; height ratio y/H = 0.5, 0.350, 0.217, 0.167, 0.083; Reynolds number Re = $2.6 \cdot 10^4$.

The heat transfer experiment was done under constant heat flux condition. This condition was maintained by supplying electrical power to the heating foils. The square prisms for heat transfer experiment were made of bakelite. Sufficient insulation was provided to minimize heat loss. Stainless steel foils 0.03 mm in thickness were used for the purpose of producing constant heat flux. The foils were polished to minimize heat loss by radiation and were connected to a copper strip on both sides through which the power was supplied. The purpose of the present investigation is to measure the local wall temperature distribution under steady-state condition at different points for calculation of both local and average heat transfer coefficients and Nusselt number. Calibrated copper-constantan thermocouples numbering 2, 3, 4, and 4 on 30, 60, 90, and 120 mm sides were embedded on each face, respectively. The positions of the thermocouples on each face of the prisms were the following: for 30 mm side prism 10, 20 mm (x/a = 0.333, 0.667); for 60 mm side 20, 30, 40 mm (x/a = 0.333, 0.5, 0.667); for 90 mm side 15, 35, 55, 75 mm (x/a = 0.167, 0.389, 0.611, 0.833); for 120 mm side 15, 45, 75, 105 mm (x/a = 0.125, 0.375, 0.625, 0.875) from the edge of each face. The copper-constantan thermocouple beads were soldered at the relevant points on the stainless steel foils. Since the size of the thermocouple beads (d = 0.5 mm) was very small, the temperature difference between the plate and surrounding air was also very small (of the order of 22–30°C). Thus, the error in the temperature measurement is also likely to be very small. This is a widely used technique for temperature measurement under constant heat flux condition. The thermocouple wires were brought out through one end-side of the prism and connected to a digital microvoltmeters via a selector switch. There is an arrangement for supplying power to different faces of the prism through a variable transformer, so that the experiment can be conducted for different heat inputs. Voltmeters and ammeters measured the voltage drop and current across the stainless steel foils, respectively.

Results and Discussion. The value of the Reynolds number (Re = ua/ν_a) was taken to be $2.6 \cdot 10^4$ in all the cases considered.

Fluid flow. The characteristics of fluid flow around a square prism were studied by measuring the pressure distribution on different faces of the prism, i.e., for different values of x/H. From the results it is observed that the pressure distribution varies with the size of the prism (i.e., with a/H) as well as with the position of the bluff body with respect to the upper wall. It was found that the pressure distribution varies considerably with the angle of attack.

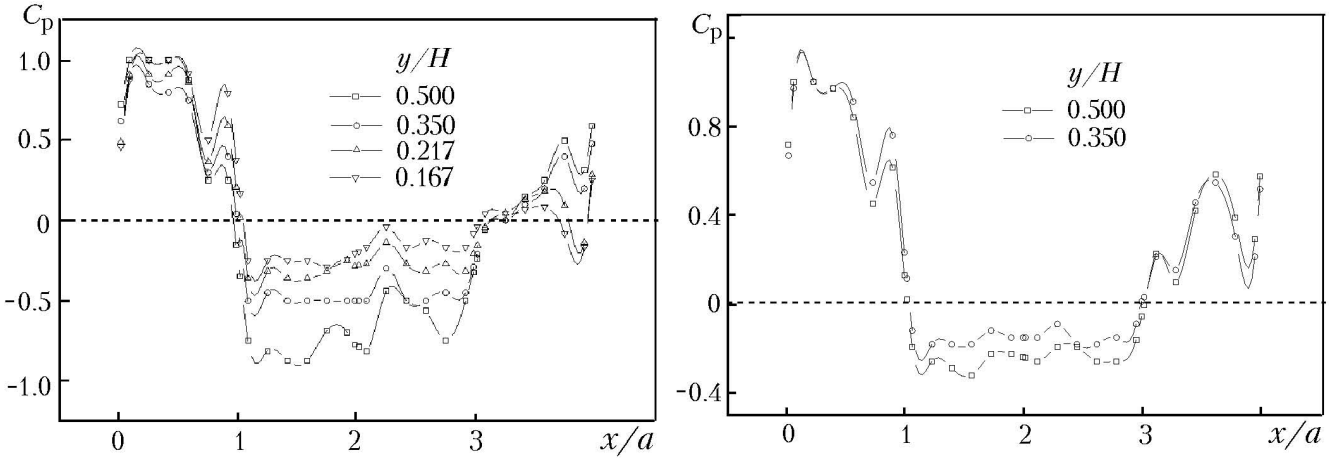

Fig. 7. Same as Fig. 6 at $a/H = 0.2$.

Fig. 8. Same as Fig. 6 at $a/H = 0.3$.

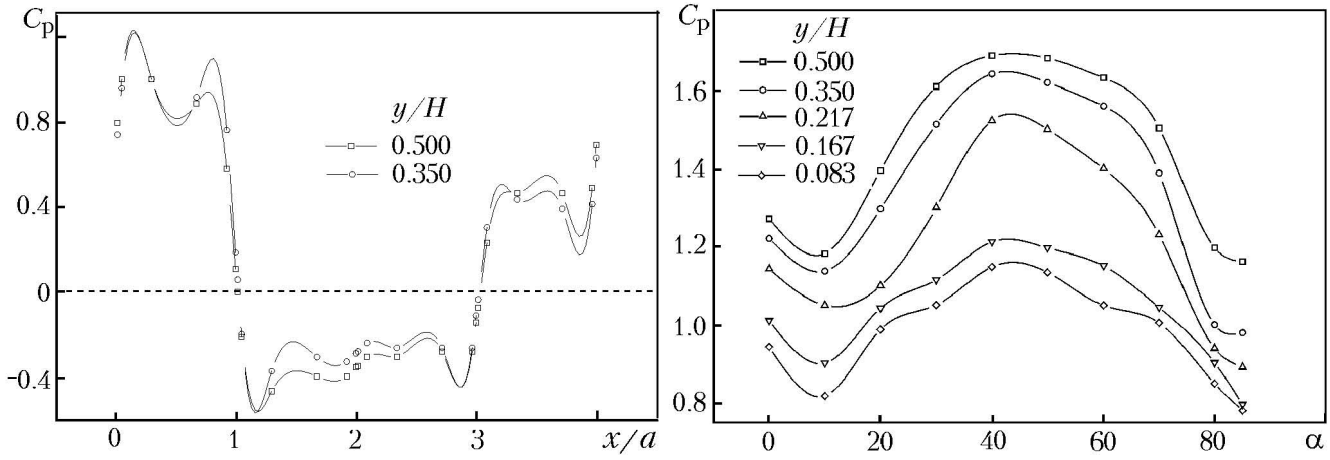

Fig. 9. Same as Fig. 6 at $a/H = 0.4$.

Fig. 10. Variation of drag coefficient with angle of attack at $a/H = 0.1$ and different height ratios of a square prism.

For determination of the pressure coefficient C_p, the pressure difference $p - p_a$ was made dimensionless by dividing by $0.5\rho_a u^2$. As the air flows over the prism, the front face, shows a positive pressure coefficient and the flow separation occurs at the rear face, causing a negative pressure coefficient. Figures 5–9 show the variation of the pressure coefficient with the dimensionless distance at different height ratios. In Fig. 5 for $\alpha = 0^o$ and $a/H = 0.1$ positive values of C_p at the front face, with respect to flow direction are almost the same for all y/H, but negative values of C_p have distinct variations for $y/H = 0.217$, 0.167, and 0.083 at some points of the surface. For $\alpha = 30^o$ (Fig. 6) almost the same behavior is found for negative values of C_p, and there are only small variations for positive values of C_p at different y/H. The flow reattaches at the lower side face, giving positive values of C_p. In Fig. 7 for the blockage ratio $a/H = 0.2$ and $\alpha = 30^o$ the negative values of pressure coefficient show a marked difference for all points of pressure tapping for different values of height ratio. Figure 8 for $a/H = 0.3$ and $\alpha = 30^o$ is closely analogous to Fig. 6. From Fig. 9 for $a/H = 0.4$ and $\alpha = 30^o$ it is observed that the positive values of C_p are almost the same for $y/H = 0.5$ and 0.350, but the negative values are slightly higher for the latter value of y/H.

The drag force F_d was calculated by integrating the pressure distribution in the direction of airflow on the four faces of the square prism. For calculation of the drag coefficient C_d, the drag force F_d was divided by $0.5\rho_a u^2 A$. Figures 10–13 show the variation of the drag coefficient with the angle of attack for different height ratios at different values of a/H. From Fig. 10 for $a/H = 0.1$ it is seen that for all y/H the drag coefficient C_d is maximum at an angle

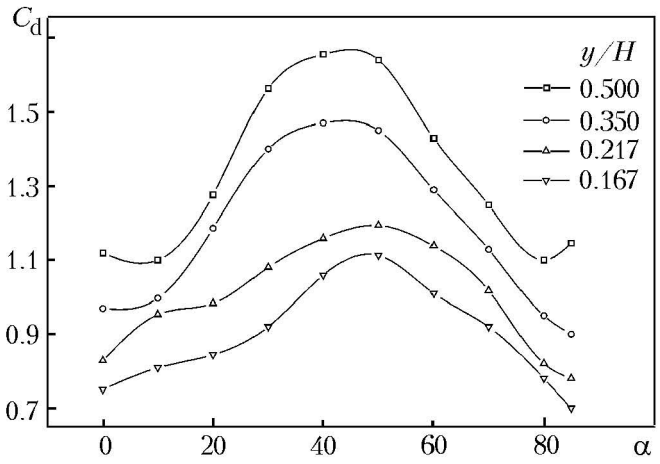

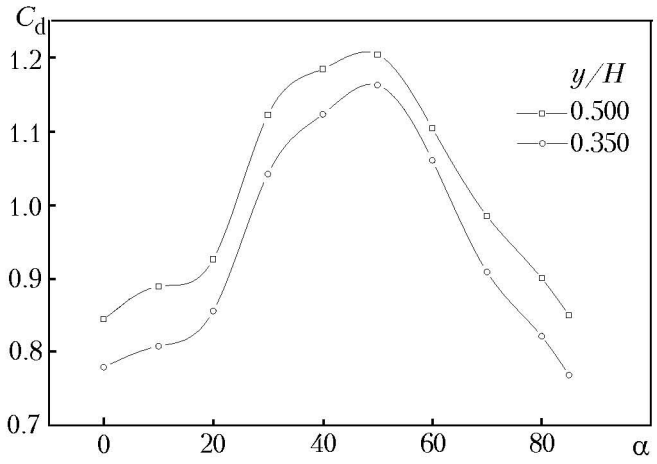

Fig. 11. Same as Fig. 10 at a/H = 0.2.

Fig. 12. Same as Fig. 10 at a/H = 0.3.

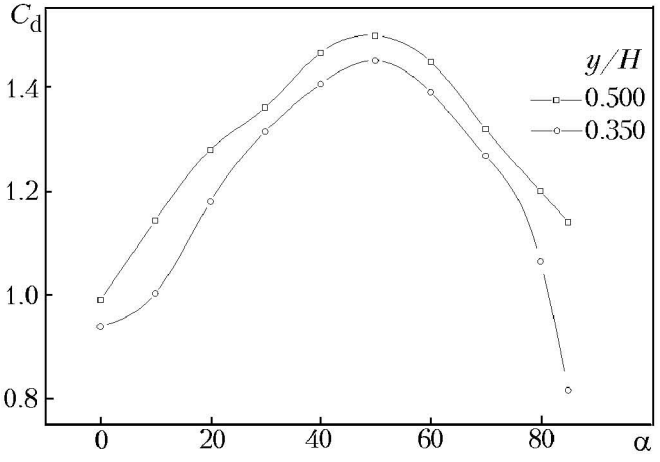

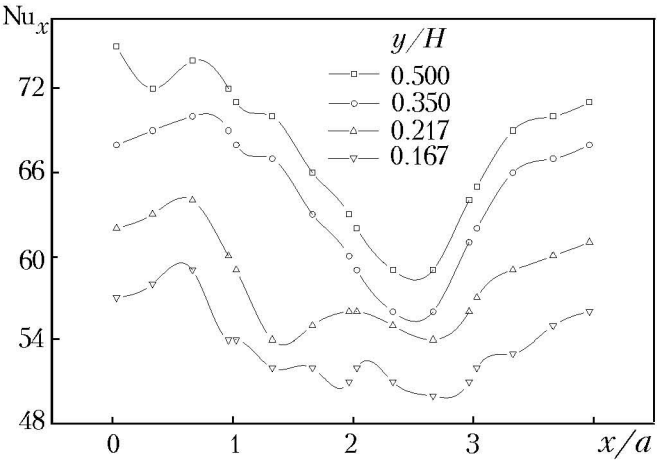

Fig. 13. Same as Fig. 10 at a/H = 0.4.

Fig. 14. Variation of local Nusselt number with dimensionless distance at a/H = 0.1, $\alpha = 0^o$, and different height ratios of a square prism.

of attack of about 50^o. For y/H = 0.167 and 0.083 the variation is not as sharp as that for other values of y/H. It is also observed that as y/H decreases, the value of C_d also decreases for all angles of attack, and when the body approaches the upper wall, the value of the drag coefficient decreases too. Figures 11–13 for other values of a/H enable one to conclude that the character of the curves is the same as in Fig. 10 and their maxima take place also at 50^o because in that orientation the area of the bluff body (i.e., square prism) is under the maximum separation zone.

From all the figures it is observed that when the body approaches the upper wall, the negative pressure coefficient decreases in magnitude and the drag coefficient for all the angles of attack also decreases. It is precisely due to the interaction with the boundary layer on the upper wall of the wind tunnel that the streamline pattern changes and the area under the separation zone at the rear side as well as at the upper face of the bluff body decreases.

The uncertainties in the determination of Re and C_p were calculated following the method given by Kline and McClintock [21] and were found to be within the range of ±3.13% and ±4.25%, respectively.

Heat transfer. Information regarding the heat transfer rate from the bluff bodies is of interest for designers in engineering practice. In the present investigation, experiments were conducted for various sizes of square prisms under constant heat flux condition. Heat flux was calculated from the heat input divided by the surface area of the heating foil. Input heat flux was corrected by subtracting the heat loss per unit area. Heat loss calculation was made by using the empirical correlation given by Hossain and Brahma [20]. The side length of a prism was taken as the characteristic

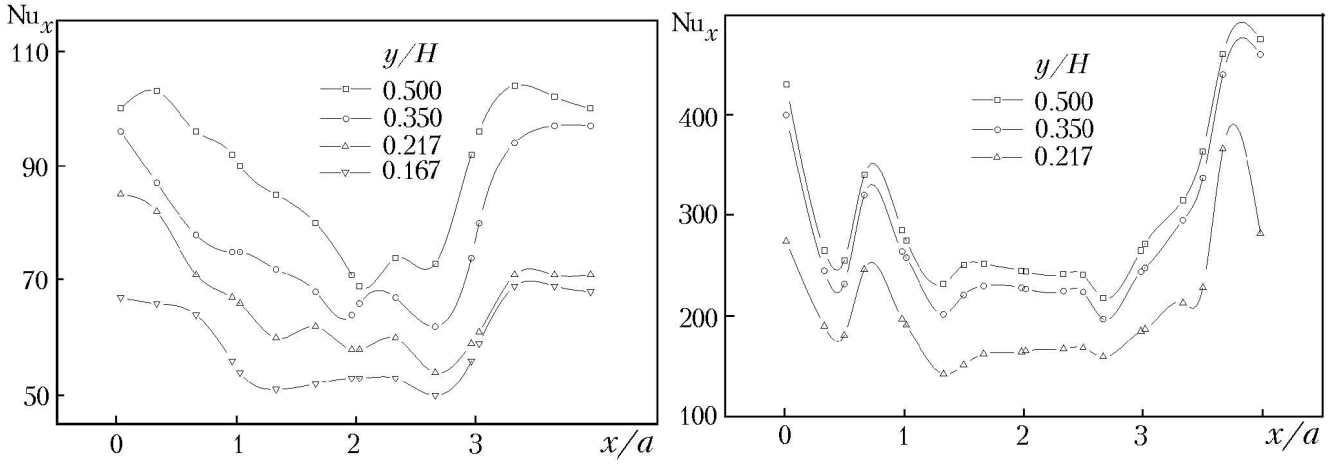

Fig. 15. Variation of local Nusselt number with dimensionless distance at a/H = 0.1, $\alpha = 30^{o}$, and different height ratios of a square prism.

Fig. 16. Same as Fig. 15 at a/H = 0.2.

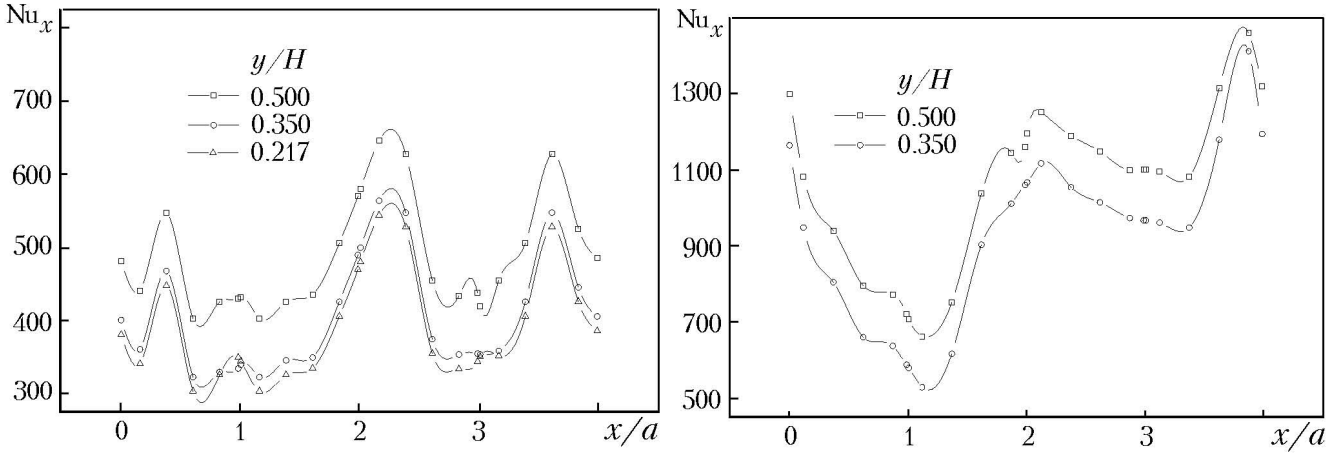

Fig. 17. Same as Fig. 15 at a/H = 0.3.

Fig. 18. Same as Fig. 15 at a/H = 0.4.

length for the definition of the local and average Nusselt number: $Nu_x = h_x a/k$, $Nu_a = h_a a/k$. The Nusselt numbers are presented for various angles of attack, blockage ratios, and height ratios for different square prisms in Figs. 14–22. Figures 14 and 15 show the variation of the local Nusselt number Nu_x with the dimensionless distance x/a at a/H = 0.1 and $\alpha = 0$ and 30^{o}, respectively. It is seen from Fig. 14 (as well as from the other graphs for Nu_x) that the local Nusselt number at all points on the surface decreases as the prism approaches the upper wall, i.e., as y/H decreases. Figure 15 for $\alpha = 30^{o}$ is almost the same as Fig. 14. Figure 16 shows the variation of Nu_x vs. x/a for a/H = 0.2. Here, the curves first sharply decrease, then increase, but within some range (namely, when x/a = 1.667–2.5) the graphs are almost straight lines and then increase sharply. Figure 17 shows the plot of the local Nusselt number for a/H = 0.3. It is seen that the curves sharply increase and decrease at some points and the difference between the results for different height ratios is insignificant. In Fig. 17 the value of Nu_x for all y/H is maximum at x/a = 2.167. Figure 18 shows Nu_x vs. x/a at a/H = 0.4. Here, the values of the local Nusselt number are minimum at x/a = 1.0083 and maximum at x/a = 3.875 for both values of y/H.

The average Nusselt numbers were calculated by the following procedure. First the values of Nu_x were integrated for all four faces separately and then added and divided by 4. Figures 19 and 20 show Nu_a vs. α for different height ratios and blockage ratios equal to 0.1 and 0.2, respectively. The maximum value of Nu_a was observed at $\alpha \sim 70^{o}$ for both cases. Figures 21 and 22 present $Nu_a(\alpha)$ for a/H equal to 0.3 and 0.4, respectively. From Fig. 21 it

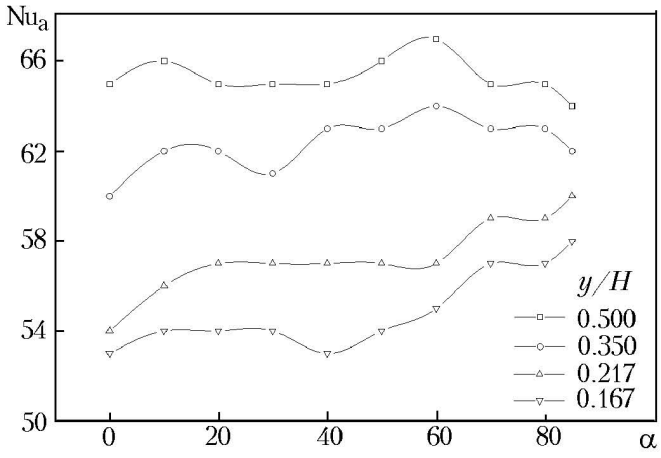

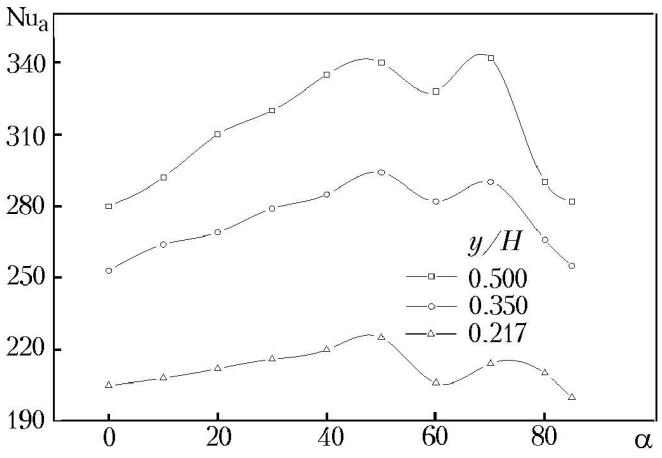

Fig. 19. Variation of average Nusselt number with angle of attack at a/H = 0.1 and different height ratios of a square prism.

Fig. 20. Same as Fig. 19 at a/H = 0.2.

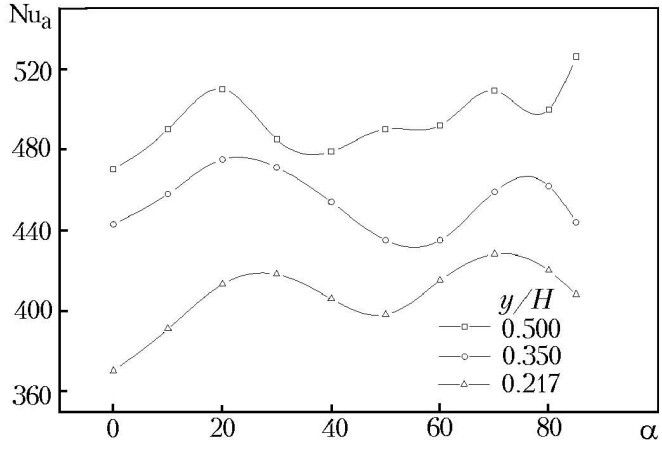

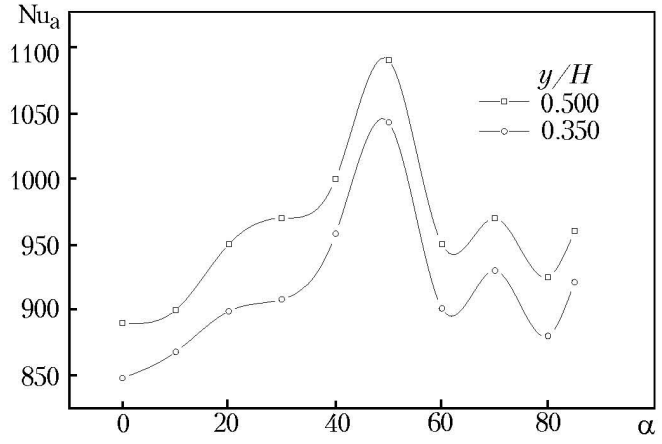

Fig. 21. Same as Fig. 19 at a/H = 0.3.

Fig. 22. Same as Fig. 19 at a/H = 0.4.

is seen that Nu_a increases up to $\alpha = 20^o$, then decreases, and again increases. The maximum value of Nu_a in Fig. 22 is observed at $\alpha = 50^o$ for both values of height ratio. In all the figures for changes of the Nusselt number with the angle of attack, the average value of Nu_a for all α decreases as the square prism approaches the upper wall, i.e., as y/H decreases.

The value of the local heat transfer coefficient decreases when the body approaches the upper wall of the wind tunnel as the area under separation zone decreases. However, it is really difficult to explain the characteristics of heat transfer phenomena under flow separation zone. Basically they depend upon the quantities described by *the local fluid mechanics*, i.e., upon velocity and static pressure distributions at a particular location at that moment.

The uncertainties in the determination of the local heat transfer coefficient and local Nusselt number were calculated according to [21] and found to be within the range ±4.52 % and ±5.25%, respectively.

CONCLUSIONS

1. The pressure coefficient C_p has positive values on the front face, whereas the rear face is within the separated flow region for all angles of attack.

2. The positive values of the pressure coefficients for all blockage ratios are almost the same at all points on the surface of prisms at different height ratios.

3. The negative values of the pressure coefficients for all blockage ratios increase for almost all points on the surface as the bluff body approaches the upper wall of the wind tunnel.

4. The values of the drag coefficient C_d for all angles of attack and blockage ratios decrease as the prism moves in the direction of the upper wall of the wind tunnel.

5. The maximum value of the drag coefficient is observed at an angle of attack of about 50^o for all blockage ratios.

6. The local Nusselt number Nu_x for all blockage ratios decreases at almost all points on the surface as the prism approaches the upper wall of the wind tunnel.

7. The values of the average Nusselt number Nu_a for all angles of attack and blockage ratios decrease as the prism moves in the direction of the upper wall of the wind tunnel.

8. There is no definite angle of attack for all blockage ratios at which the value of the average Nusselt number is either maximum or minimum.

NOTATION

a, side length of a square prism, mm; a/H, blockage ratio; A, surface area of a bluff body, m^2; C_d, drag coefficient; C_p, pressure coefficient; d, size of thermocouple beads, mm; F_d, drag force, N; h_x, local heat transfer coefficient, $W/(m^2 \cdot K)$; h_a, average heat transfer coefficient, $W/(m^2 \cdot K)$; H, height of the wind tunnel, mm; k, thermal conductivity, $W/(m \cdot K)$; Nu_x, local Nusselt number; Nu_a, average Nusselt number; p, static pressure, mm of water; p_a, ambient pressure, mm of water; Re, Reynolds number; u, velocity of airflow, m/sec; x, distance along the prism perimeter starting from the corner A in Fig. 1, mm; y, distance of the centroid of a bluff body from the upper wall of the wind tunnel, mm; α, angle of attack, ^{o}; ρ_a, density of air, kg/m^3; ν_a, kinematic viscosity of air, m^2/sec.

REFERENCES

1. P. W. Bearman, Investigation of flow behind a two-dimensional model with blunt trailing edge and fitted with splitter plates, *J. Fluid Mech.*, **21**, No. 2, 241–255 (1965).
2. P. W. Bearman and D. M. Trueman, An investigation of the flow around rectangular cylinders, *Aeronaut. Quart.,* **23**, 229–237 (1972).
3. C. J. Aplet et al., The effects of wake splitter plates on the flow past a circular cylinder in the range $10^4 < Re < 5 \times 10^4$, *J. Fluid Mech.*, **61**, No. 1, 187–198 (1973).
4. P. W. Bearman and M. M. Zdravkovich, Flow around a circular cylinder near a plane boundary, *J. Fluid Mech.*, **89**, No. 1, 53–73 (1978).
5. T. Igarashi, Characteristics of the flow around a square prism, *Bull. JSME*, **27**, 1858–1864 (1984).
6. T. Igarashi, Characteristics of flow around rectangular cylinders, *Bull. JSME*, **28**, 1690–1696 (1985).
7. V. Mansingh and P. H. Oosthuizen, Effects of splitter plates in the wake flow behind a bluff body, *AIAA J.*, **28**, 778–783 (1990).
8. R. L. Simpson, The structure of the near wall region of two-dimensional turbulent separated flow, *Philos. Trans. R. Soc.* London, **336**, 5–7 (1991).
9. T. Igarashi, Heat transfer in separated flows, in: *Proc. 5th International Heat Transfer Conference*, Tokyo (1974), pp. 300–304.
10. T. Igarashi et al., Heat transfer in separated flows. Part 1. Experiments on local heat transfer from the rear of a flat plate to an air stream, *Heat Transf. Jap. Res.*, **4**, No. 1, 11–32 (1975).
11. T. Igarashi and M. Hirata, Heat transfer in separated flows. Part 3. The case of equilateral triangular prisms, *Heat Transf. Jap. Res.*, **6**, No. 4, 13–39 (1977).
12. T. Igarashi, Heat transfer in separated flows. Part 2. Theoretical analysis, *Heat Transf. Jap. Res.*, **6**, No. 3, 60–78 (1977).
13. T. Igarashi, Fluid flow and heat transfer in the separated region of a circular cylinder with wake control, *Heat Transf. Jap. Res.,* **11**, No. 3, 1–16 (1982).

14. T. Igarashi, Correlation between heat transfer and fluctuating pressure in separated region of a circular cylinder, *Int. J. Heat Mass Transf.*, **27**, No. 6, 927–937 (1984).
15. T. Igarashi, Heat transfer from a square prism to an air stream, *Int. J. Heat Mass Transf.,* **28**, No. 1, 175–181 (1985).
16. S. Aiba and H. Tsuchoda, Heat Transfer around a circular cylinder near a plane boundary, *Trans JSME*, 51–463, 866–873 (1985).
17. T. Igarashi, Local heat transfer from a square prism to an air stream, *Int. J. Heat Mass Transf.,* **29**, No. 5, 777–784 (1986).
18. T. Igarashi, Fluid flow and heat transfer around rectangular cylinders, *Int. J. Heat Mass Transf.*, **30**, No. 5, 893–901 (1987).
19. M. M. Yovanovich and G. Refai-Ahmed, Experimental study of forced convection from isothermal circular and square cylinders and toroids, *J. Heat Transf., Trans. ASME*, **119**, 70–79 (February 1997).
20. A. Hossain and R. K. Brahma, Experimental investigations of fluid flow and heat transfer characteristics of a slot jet impinging on a square cylinder, *Wärme- und Stoffübertragung*, **28**, 381–386 (1993).
21. S. J. Kline and F. A. McClintock, Describing uncertainties in single-sample experiments, *Mech. Eng.*, **75**, 3–8 (1953).